Local Measurements of Correlated Momentum and Heat Transport in the TFTR Tokamak

S. D. Scott, P. H. Diamond,[a] R. J. Fonck,[b] R. J. Goldston, R. B. Howell,[c] K. P. Jaehnig, G. Schilling, E. J. Synakowski, M. C. Zarnstorff, C. E. Bush,[d] E. Fredrickson, K. W. Hill, A. C. Janos, D. K. Mansfield, D. K. Owens, H. Park, G. Pautasso,[e] A. T. Ramsey, J. Schivell, G. D. Tait, W. M. Tang, and G. Taylor

Plasma Physics Laboratory, Princeton University, Princeton, New Jersey 08543

(Received 10 August 1989)

Simultaneous profile measurements of the toroidal rotation speed and ion temperature during unbalanced neutral-beam injection in the Tokamak Fusion Test Reactor show that the ion momentum and thermal diffusivities are comparable in magnitude ($\chi_\phi \approx 1.5\chi_i$) and vary similarly with plasma current and minor radius. The correlation of χ_ϕ and χ_i is consistent with anomalous transport driven by collisionless electrostatic microinstabilities including ion-temperature-gradient–driven modes (η_i modes) and collisionless trapped-electron modes.

PACS numbers: 52.25.Fi, 52.50.Gj, 52.55.Fa

The toroidal rotation speeds attained in tokamak plasmas during neutral-beam heating are universally observed to be very small compared to predictions based on calculated beam torques and classical perpendicular viscosity. Many tokamaks have reported similar magnitudes for the global momentum and energy confinement times, or similar scalings of these times with plasma conditions.[1] Measurements of the ion-temperature profile on D-III[2] and TFTR[3] have revealed narrower profiles than would be expected from neoclassical ion heat transport, implying anomalous ion heat transport ($\chi_i \gg \chi_i^{\text{neo}}$). These observations motivated an experimental study to determine the correlation between local transport coefficients for momentum and thermal diffusivity. There is considerable theoretical interest in such correlations, because the ion-temperature-gradient–driven class of instabilities (η_i modes), which have been identified as potential candidates for explaining the rapid heat transport in tokamaks,[4] produce equal levels of ion heat and momentum diffusivity ($\chi_\phi = \chi_i$),[5] as do all models of electrostatic turbulence in which the ion response is hydrodynamic. Moreover, very recent studies of collisionless trapped-electron modes[6] (CTEM) have indicated $\chi_\phi \approx \chi_i \approx \chi_e$.

In this Letter we discuss a transport analysis of rotation and ion-temperature profiles on TFTR which indicates a strong correlation between radial transport of momentum and heat. The profile measurements were performed at $B_T = 4.8$ T in a series of four neutral-beam power scans (4.4–15 MW) at two values of plasma current (1.1 and 1.7–1.8 MA) using either co- or counter-only tangential neutral-beam injection ($R_{\text{tan}} = 1.7$–2.3 m). In addition, a toroidal-field scan was performed for $I_p = 1.0$ MA at $B_T = 2.9$, 3.8, and 4.8 T using separately 7 MW of co-beam power and 12 MW of counter-beam power. The ion-temperature and toroidal-rotation-speed measurements were obtained by charge-exchange recombination spectroscopy with 5-cm spatial resolution, when the plasma density and stored energy had reached quasi-steady state ($N_e/\dot{N}_e \geq 1.5$ sec, and $W_{\text{tot}}/\dot{W}_{\text{tot}} \geq 1.2$ sec). Deuterium-neutral-beam injection ($E_{\text{inj}} \approx 105$ keV) into deuterium target plasmas was utilized in all discharges, with the plasma resting against a low-recycling inner bumper limiter[7] ($R = 2.45$ m, and $a = 0.79$ m).

During co-injection, high central ion temperatures [$T_i(0) \leq 23$ keV] and rotation speeds [$v_\phi(0) \leq 5.7 \times 10^5$ m/s] were achieved at modest plasma densities [$\bar{n}_e = (1.0$–$2.8) \times 10^{19}$ m^{-3}]. The electron-density peakedness [$F_{ne} \equiv n_e(0)/\langle n_e \rangle$] ranged from 1.7 to 2.0, placing it roughly between typical L-mode and Supershot values.[8] During co-injection, the global energy confinement times from magnetic measurements of the total stored energy gave $\tau_E/\tau_E^{L\,\text{mode}}$ ranging from 1.1 to 1.7, where $\tau_E^{L\,\text{mode}}$ is the expected L-mode confinement time from Ref. 9 multiplied by 1.20 to account for species scaling. Counter-injection consistently yielded higher plasma densities (by 10%–37%), but lower central ion temperatures and rotation speeds (by up to a factor of 2), and $\sim$20% lower τ_E. The density-profile peakedness was either the same or only modestly lower ($\Delta F_{ne} \leq 0.1$) during counter-injection, in contrast to results reported by ASDEX with counter-injection.[10] One characteristic feature of all the discharges in this experiment was the substantial contribution by unthermalized beam ions to the plasma density [$n_{\text{fast}}(0)/n_e(0) = 0.10$–$0.40$], stored momentum ($L_{\text{fast}}/L_{\text{tot}} = 0.50$–$0.75$), and stored energy ($W_{\text{fast}}/W_{\text{tot}} = 0.40$–$0.70$).

The particle, momentum, and energy transport in these plasmas have been analyzed using the 1D steady-state transport analysis code SNAP based on the experimentally measured density, velocity, and temperature profiles. $T_e(r)$ was measured by electron-cyclotron emission and $n_e(r,t)$ by a ten-channel infared interferometer. The ion depletion was calculated using tangential visible-bremsstrahlung measurements for Z_{eff} ($= 2.8$–4.3) and x-ray spectroscopic measurements of metallic concentrations [$Z_{\text{eff}}(\text{metals}) = 0.2$–$1.1$], assuming Z_{eff} to be flat across the plasma cross section, consistent with preliminary measurements. Edge hydrogenic-neutral influx was inferred[11] from measurements of an array of absolutely calibrated H_α detectors. The

calculated beam deposition in the SNAP code includes ionization and charge-exchange processes by thermal ions and electrons, as well as by the slowing-down beam-ion population. The beam-ion distribution function was calculated from a solution of the Fokker-Planck equation in the rotating plasma frame,[12] neglecting radial diffusion, consistent with experimental observations at low power.[13]

The particle, momentum, and energy transport are analyzed assuming that the radial transport mechanisms are cross field diffusion, represented by anomalous diffusivities D_e, χ_ϕ, χ_i, and χ_e, radial convection due to particle flows, and charge-exchange losses, which are important for the ion power balance near the edge;

$$Q_i \equiv -\chi_i \left(\sum_j n_j\right) \nabla T_i + \tfrac{3}{2}\Gamma_i T_i \equiv -\chi_i^{\text{eff}} \left(\sum_j n_j\right) \nabla T_i ,$$

$$Q_e \equiv -\chi_e n_e \nabla T_e + \tfrac{3}{2}\Gamma_e T_e \equiv -\chi_e^{\text{eff}} n_e \nabla T_e ,$$

$$\gamma \equiv -\chi_\phi \left(\sum_j n_j m_j\right) \nabla v_\phi + \Gamma_i \langle m_h \rangle v_\phi \equiv -\chi_\phi^{\text{eff}} \left(\sum_j n_j m_j\right) \nabla v_\phi ,$$

$$\Gamma_e \equiv -D_e \nabla n_e ,$$

where Q_i and Q_e are the total ion and electron heat flux, Γ_i and Γ_e are the ion and electron particle flux (Γ_i is assumed hydrogenic with average mass $\langle m_h \rangle$), Σ_j represents a sum over all ion species including impurities, γ is the radial flux of toroidal momentum, and χ_i^{eff}, χ_e^{eff}, and χ_ϕ^{eff} are "effective" diffusivities which include both the convective and conductive fluxes. This analysis neglects pinch effects and off-diagonal terms, as well as local damping due to toroidal field ripple (which is negligible for TFTR conditions).

Ion heat convection is the dominant core transport mechanism during balanced and co-tangential injection into low-recycling plasmas,[3] which precludes a meaningful calculation of χ_i in this region (although χ_i^{eff} is still well determined). Heat conduction becomes the dominant loss channel outside this core, so the difference between χ_i^{eff} and χ_i (and χ_e^{eff} and χ_e) is less than 50% for $r/a \geq 0.4$. By contrast, the contribution of convection to the momentum balance is small throughout the plasma, so χ_ϕ^{eff} differs from χ_ϕ by less than 20% for $r/a \geq 0.2$ in all discharges. Figure 2(a) illustrates the radial dependence of χ_ϕ^{eff}, χ_i^{eff}, and χ_e^{eff} for the discharge shown in Fig. 1. There is a striking correlation between the momentum and thermal diffusivities both in magnitude and in their variation with minor radius. To establish error bars on the computed diffusivities, an ensemble of 100 transport analyses was performed, using the measured profiles [$v_\phi(R)$, $T_i(R)$, $T_e(R)$, and $n_e(R)$] and other input data (Z_{eff}, P_b, etc.) simultaneously varied within their ranges of uncertainty by Monte Carlo sampling a Gaussian distribution for both statistical and systematic errors. The error bars shown in Fig. 2 encompass 90% of the calculated diffusivity values. Velocity profiles *calculated* on the basis of $\chi_\phi \propto \chi_i^{\text{eff}}(r)$ and the measured density profile and the calculated torque deposition profile reproduce the measured velocity profiles quite well (Fig. 1); for $\chi_\phi(r) = 1.1\chi_i^{\text{eff}}(r)$, $v_{\phi-\text{calc}}(r/a = 0.2)$ is within $\pm 30\%$ of the measured velocity for all other discharges in the experiment.

The correlation between χ_ϕ^{eff}, χ_e^{eff}, and χ_i^{eff} over a wider range of plasma conditions is illustrated in Fig. 3, which shows the inferred diffusivities for all discharges in the

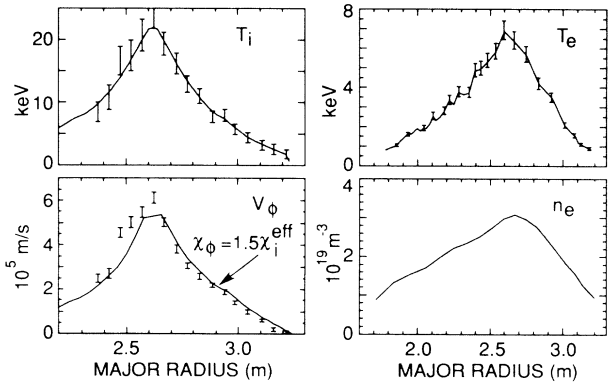

FIG. 1. Measured plasma profiles during co-injection at $P_b = 11.6$ MW. The solid line in the $v_\phi(R)$ plot represents the calculated velocity profile assuming $\chi_\phi = 1.5\chi_i^{\text{eff}}$.

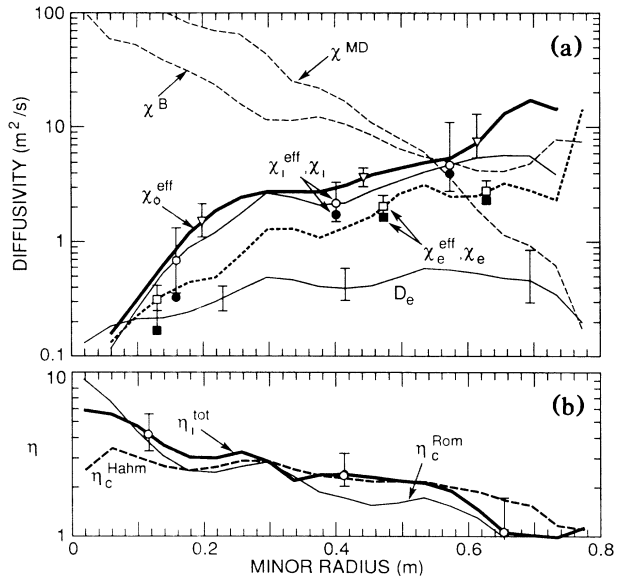

FIG. 2. (a) Experimentally determined particle diffusivity, and effective momentum and thermal diffusivities for the discharge shown in Fig. 1. The solid symbols on the curves for χ_i^{eff} and χ_e^{eff} show the corresponding values of χ_i and χ_e ($\chi_\phi^{\text{eff}} = \chi_\phi$ within $\sim 10\%$). Also shown are the theoretical χ_ϕ ($= \chi_i$) from Mattor and Diamond (Ref. 5) (labeled χ^{MD}), and the χ_i from toroidal η_i analysis of Biglari, Diamond, and Rosenbluth (Ref. 14) (labeled χ^{B}). (b) Comparison of measured η_i^{tot} with the theoretical estimates η_c^{Rom} and η_c^{Hahm}.

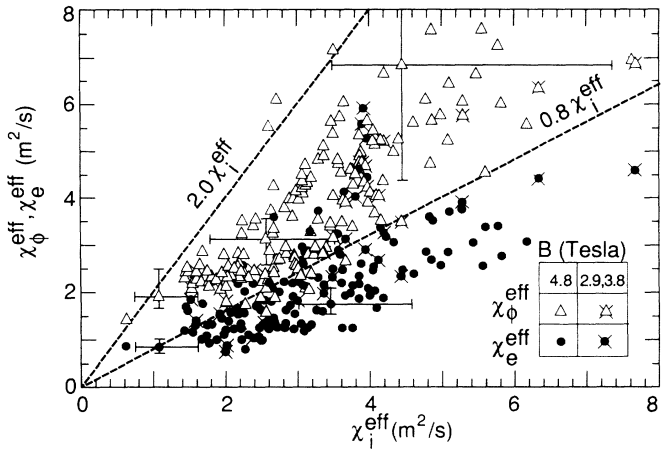

FIG. 3. Measured effective thermal and momentum diffusivities for all discharges in the experiment in the region $0.3 \leq r/a \leq 0.8$.

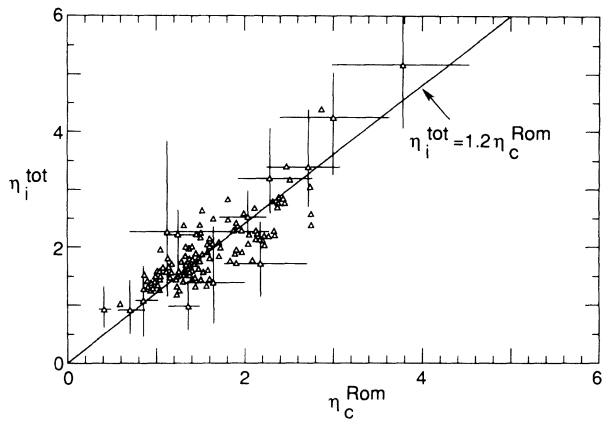

FIG. 4. Measured η_i^{tot} plotted as a function of threshold η_c^{Rom} for marginal stability of η_i modes in the region $0.3 \leq r/a \leq 0.8$. η_c^{Rom} does not incorporate potentially important effects associated with the large fast-ion population in these plasmas.

region $r/a = 0.3$–0.8. The data shown in Fig. 3 are constrained by the requirements (a) $n_i/n_e \geq 0.3$; (b) minor radius more than 10 cm beyond sawtooth-inversion radius; and (c) radiated power less than 50% of total power delivered to electrons. Note that while the plasma conditions n_e, T_e, T_i, and v_ϕ vary by factors of 4–13 across the data set, the ratios of local diffusivities (and "effective diffusivities") remain relatively constant: $\chi_\phi/\chi_i = 0.7$–2.0, $\chi_i/\chi_e = 0.8$–2.5, $\chi_\phi/\chi_e = 1.2$–3.1, and $\chi_e/D_e = 2.5$–9.0, where the quoted limits encompass $\sim 95\%$ of the data.

Most of the factor ~ 10 variation in χ_ϕ, χ_i, and χ_e shown in Fig. 3 is due to their strong dependences on minor radius; at fixed radius ($r/a = 0.5$) they each change less than a factor of 2.5 across the entire data set. Comparing discharges where only one controllable parameter (I_p, B_T, P_b, or beam direction) was changed, we find variations in χ_ϕ, χ_e, and χ_i comparable to or less than their estimated uncertainties of 20%–50%. This establishes that none of the local diffusivities are strongly dependent on these global parameters, but also precludes a precise comparison of their scaling. Nevertheless, three qualitative trends have been identified from examining the diffusivity data at $r/a = 0.5$ and from power-law regression fits to the data in the region $r/a = 0.3$–0.8: (1) χ_ϕ, χ_i, and χ_e are weakly or vanishingly dependent on B_T; (2) χ_ϕ and χ_i decrease weakly with current ($\Delta\chi = -15\%$ to -40% as I_p increases from 1.0 to 1.8 MA); and (3) χ_ϕ, χ_i, and χ_e increase strongly with minor radius. The power-law regression for

$$\chi_\phi - \chi_\phi \propto C_\phi P_b^{0.23} I_p^{-0.59} B_T^{0.16} (r/a)^{1.22}$$

($C_\phi = 1.0$ for co-injection and 1.15 for counter-injection) reproduces all of measured values of χ_ϕ in Fig. 3 within $\pm 25\%$.

A comparison of the measured diffusivities and scale lengths with predictions of η_i-mode theory is seriously compromised by the significant fast-ion population in these plasmas, which presumably affects both the stability threshold for η_i modes (and for CTEM modes) and their saturated turbulence levels, but which is not yet included in theoretical models. The large fast-ion population coupled with moderate Z_{eff} yields small ratios of n_i^{th}/n_e ($= 0.1$–0.5 at the plasma center) and correspondingly a large uncertainty in the radial profiles of thermal ion density, which are typically calculated to be flat or inverted over most of the plasma cross section despite peaked $n_e(r)$ profiles. Accordingly, we adopt a coarse view by including fast ions in the definition of η_i, $\eta_i^{tot} \equiv d\ln T_i/d\ln(n_i^{th} + n_b)$. Figure 2(a) compares the measured χ_ϕ^{eff} and χ_i^{eff} to two standard theoretical models[5,14] of ion-temperature-gradient-driven transport. Inside $r/a = 0.7$, the theoretical diffusivities are considerably larger than the experimental values. The potential strength of η_i transport therefore suggests that the observed profiles might be regulated by marginal stability,[15] which would impose $\eta_i \approx \eta_c$ on the plasmas by rapidly relaxing $T_i(R)$ whenever the threshold η_c was temporarily exceeded.

The gradient scale lengths in these plasmas span the ranges $L_v (\equiv \partial \ln v/\partial \ln r) = 0.1$–$0.6$ m, $L_{T_i} = 0.2$–0.6 m, $L_{n_i^{tot}} [\equiv \partial \ln(n_i^{th} + n_b)/\partial \ln r] = 0.3$–$1.2$ m, and $\eta_i^{tot} = 0.8$–4.5. Figure 2(b) shows two theoretical estimates of the threshold η_c by Romanelli[16] and by Hahm and Tang[17] which are within a factor of 2 of the measured η_i^{tot}. There is considerable scatter in a plot of η_i^{tot} vs η_c^{Rom} (Fig. 4) for all the discharges in the experiment, spanning a factor of 2 in η_i^{tot} for fixed η_c. The data of Fig. 4 are nevertheless suggestive of a correlation between η_c^{Rom} and η_i^{tot}. In particular, the highest and lowest η_i^{tot} correspond to the highest and lowest η_c^{Rom}, and $\sim 98\%$ of the measured values of η_i^{tot} lie within one error "box" of the line $\eta_i^{tot} = 1.2\eta_c^{Rom}$.

In summary, by simultaneously measuring $v_\phi(R)$, $T_i(R)$, $T_e(R)$, and $n_e(R)$ during strong unidirectional beam injection on TFTR, we have demonstrated a strong correlation between the radial transport of momentum and heat in low-recycling plasmas. The measured ratios of χ_ϕ/χ_i and χ_e/χ_i are in reasonable agreement with predictions based on theoretical models of electrostatic turbulence. The observed gradient scale lengths for T_i and η_i^{tot} are roughly those expected for a plasma at marginal stability to strong η_i-mode transport, although it must be stressed that the theory has not yet addressed potentially important effects of a suprathermal ion population which is large in the plasma regime studied here (leading to significant fast-ion contributions to total plasma energy and momentum, and low n_i^{th}/n_e). These results provide some experimental basis for the supposition that collisionless electrostatic microinstabilities (η_i modes or CTEM modes) are the dominant mechanism for heat and momentum transport in these plamas.

It is a pleasure to acknowledge the many physicists, engineers, technicians, and other staff members who have supported the TFTR program. We are grateful to H. Biglari and J. D. Callen for useful discussions, and to D. C. McCune, J. A. Murphy, H. H. Towner, and R. M. Wieland for computational support. This work was supported by the U.S. DOE, Contract No. DE-AC02-76-CHO-3073.

[a]Permanent address: University of California at San Diego, La Jolla, CA 92093.

[b]Permanent address: University of Wisconsin, Madison, WI 53706.

[c]Permanent address: Massachusetts Institute of Technology, Cambridge, MA 02139.

[d]Permanent address: Oak Ridge National Laboratory, Oak Ridge, TN 37830.

[e]Permanent address: Georgia Institute of Technology, Atlanta, GA 30332.

[1]S. Suckewer *et al.*, Nucl. Fusion **21**, 1301 (1981); K. Brau *et al.*, Nucl. Fusion **23**, 1643 (1983); N. Hawkes and N. Peacock, Nucl. Fusion **25**, 971 (1985); R. C. Isler *et al.*, Nucl. Fusion **26**, 391 (1986); K. Burrell, R. Groebner, H. S. John, and R. Seraydarian, Nucl. Fusion **28**, 3 (1988).

[2]R. Groebner *et al.*, Nucl Fusion **26**, 543 (1986).

[3]R. Fonck *et al.*, Phys. Rev. Lett. **63**, 520 (1989); M. Zarnstorff *et al.*, in *Proceedings of the Twelfth International Conference on Plasma Physics and Controlled Nuclear Fusion Research, Nice, France, 1988* (International Atomic Energy Agency, Vienna, 1989), Vol. 1, p. 183.

[4]B. Coppi, M. N., Rosenbluth, and R. Z. Sagdeev, Phys. Fluids **10**, 582 (1967); W. Tang, Nucl. Fusion **26**, 1605 (1986); F. Romanelli, W. Tang, and R. White, Nucl. Fusion **26**, 1515 (1986); R. Dominguez and R. Waltz, Nucl. Fusion **27**, 65 (1987); G. Lee and P. Diamond, Phys. Fluids **29**, 3291 (1986).

[5]N. Mattor and P. Diamond, Phys. Fluids **31**, 1180 (1988).

[6]T. Hahm and W. Tang, contribution to the Sherwood Controlled Fusion Theory Conference, San Antonio, 1989 (unpublished), paper 3C8.

[7]H. Dylla *et al.*, Nucl Fusion **27**, 1221 (1987).

[8]H. Park *et al.*, Princton Plasma Physics Laboratory Report No. PPPL-2651, 1989 (to be published); M. G. Bell *et al.*, in *Proceedings of the Twelfth International Conference on Plasma Physics and Controlled Nuclear Fusion Research, Nice, France, 1988* (International Atomic Energy Agency, Vienna, 1989), Vol. 1, p. 27.

[9]R. Goldston, Plasma Phys. Controlled Fusion **26**, 87 (1984).

[10]O. Gehre *et al.*, Phys. Rev. Lett. **60**, 1502 (1988).

[11]D. H. Heifetz *et al.*, J. Vac. Sci. Technol. A **6**, 2564 (1988).

[12]R. Goldston, in *Proceedings of the Course and Workshop on Basic Physical Processes of Toroidal Fusion Plasmas, Varenna, Italy, 1985,* International School of Physics "Piero Caldirola," edited by G. P. Lampis *et al.* (Monotypia Franchi, Citta di Castello, Italy, 1985), p. 165.

[13]R. Radeztsky *et al.*, in *Proceedings of the Fifteenth European Conference on Controlled Fusion and Plasma Physics, Dubrovnik, Yugoslavia, 1988,* edited by N. Cindro, R. Caplar, and J. Jacquinot (European Physical Society, Petit-Lancy, Switzerland, 1988), p. 79; P. C. Efthimion *et al.*, in *Proceedings of the Twelfth International Conference on Plasma Physics on Controlled Nuclear Fusion, Nice, France, 1988* (International Atomic Energy Agency, Vienna, 1989), Vol. 1, p. 307.

[14]H. Biglari, P. Diamond, and M. Rosenbluth, Phys. Fluids B **1**, 109 (1989), Eq. (22).

[15]H. Biglari *et al.*, in *Proceedings of the Twelfth International Conference on Plasma Physics and Controlled Nuclear Fusion Research, Nice, France, 1988* (International Atomic Energy Agency, Vienna, 1989), Vol. 2, p. 261.

[16]F. Romanelli, Phys. Fluids B **1**, 1018 (1989), Eq. (26).

[17]T. Hahm and W. Tang, Phys. Fluids B **1**, 1185 (1989), Eqs. (8) and (11).